Bull. Mater. Sci., Vol. 34, No. 5, August 2011, pp. 1039–1048. © Indian Academy of Sciences.

Preparation and investigation of Al–4 wt % B_4C nanocomposite powders using mechanical milling

A ALIZADEH, E TAHERI-NASSAJ* and H R BAHARVANDI†
Department of Materials Science and Engineering, Tarbiat Modares University, PO Box 14115-143, Tehran, Iran
†MUT University, PO Box 15875-1774, Tehran, Iran

MS received 10 November 2010; revised 8 February 2011

Abstract. Boron carbide nanoparticles were produced using commercially available boron carbide powder (0·8 μm). Mechanical milling was used to synthesize Al nanostructured powder in a planetary ball-mill under argon atmosphere up to 20 h. The same process was applied for Al–4 wt % B_4C nanocomposite powders to explore the role of nanosize reinforcements on mechanical milling stages. Scanning electron microscopy (SEM) analysis as well as apparent density measurements were used to optimize the milling time needed for completion of the mechanical milling process. The results show that the addition of boron carbide particles accelerate the milling process, leading to a faster work hardening rate and fracture of aluminum matrix. FE-SEM images show that distribution of boron carbide particles in aluminum matrix reaches a full homogeneity when steady state takes place. The better distribution of reinforcement throughout the matrix would increase hardness of the powder. To study the compressibility of milled powder, modified heckel equation was used to consider the pressure effect on yield strength as well as reinforcing role of B_4C particles. For better distribution of reinforcement throughout the matrix, *r*, modified heckel equation was used to consider the pressure effect on yield strength as well as reinforcing role of B_4C particles.

Keywords. Boron carbide nanoparticles; mechanical milling; Al–B_4C nanocomposite powders; compressibility.

1. Introduction

Metal matrix composites (MMCs) have considerable applications in aerospace, automotive and military industries due to their high mechanical properties and good physical behaviour including light weight, electrical and thermal conductivity (Boey *et al* 1998; Parvin *et al* 2008).

Powder metallurgy is among the most important processing techniques used for manufacture of metal matrix composites (MMCs). It can eliminate reinforcement segregation that generally takes place in casting process. Segregation severely affects MMC properties and thus is effective for improving the mechanical properties and also other properties (Gan and Gu 2006). Factors such as different particle sizes, density, geometries, flow or the development of an electrical charge during mixing may lead to agglomeration (Fogagnolo *et al* 2006). In this process, mixing of matrix and reinforcement is a critical step to obtain a homogenous distribution of reinforcing particles in matrix.

Since by reducing ceramic particle size the stress concentration level on each particle is decreased and makes it difficult to be fractured, nanoscale ceramic particles have attracted attention both in academia and industry (Zhang *et al* 2004; Liua *et al* 2009).

*Author for correspondence (taheri@modares.ac.ir)

Various mechanical methods like high energy processes such as planetary, attrition and jet milling are available to prepare ultra fine particles (Aparecida *et al* 2006). Attrition mill has been widely used for fine grinding of different materials. The main advantages of attrition mills are relatively high energy utilization, fast and efficient fine grinding and simple operation (Shinohara *et al* 1999). Due to high activeness and proneness to agglomeration of nanoparticles, one major challenge to manufacture nanocomposites is how the reinforcing particles disperse homogenously throughout the matrix (Liua *et al* 2009). One way to improve particle distribution is using mechanical alloying technique (MA) or ball milling process.

During MA two essential processes are involved, viz. cold welding and fracturing of powder particles. The constituent powder particles are repeatedly cold welded and fractured so that powder particles having ultra fine structure are produced after MA. The advantage of MA to manufacture composite powder with a homogenous distribution of particles throughout the matrix has resulted in the synthesis of nanocomposite systems like Al/CNT (Wang *et al* 2009), Al/Al_2O_3 (Razavi Hesabi *et al* 2006), Al/graphite (Mndoza-Ruiz *et al* 2008), and Al/SiC (Saberi *et al* 2009).

Although there are so many metallic alloy systems which can be used as matrix, most attempts have been concentrated on Al alloys due to their low density, heat treatment capability, wide range of its alloys and processing flexibility.

Recently, B_4C reinforced composites have been manufactured via various techniques (Hu *et al* 2001; Zhang *et al* 2004; Jiang *et al* 2005; Kerti and Toptan 2008; Mohanty *et al* 2008). B_4C is the third hardest material after diamond and CBN. Furthermore, B_4C has a lower specific gravity (2·51 g/cm^3 which is less than Al with 2·7 g/cm^3), high wear and impact resistance, high melting point, good resistance to chemical agents and high capacity for neutron absorption. B_4C is a proper candidate as reinforcement in Al matrix composites (Alizadeh *et al* 2004; Ye *et al* 2006). It can be considered as an alternative to SiC reinforced composites where a high stiffness or a good wear resistance is required (Onoro *et al* 2009).

This study is aimed at using synthesized nanoscaled particles of B_4C to produce Al–4 wt % B_4C nanocomposite and investigation of the role of B_4C nanoparticles on structural evolution during MA. Changes like crystal size, lattice strain matrix alloy and microhardness in different periods have been studied. Also the effect of reinforcement on the compressibility of milled powder has been investigated.

2. Experimental

Argon gas atomized Al–2 wt % Cu powders with a mean size of 27 μm were used as the matrix alloy.

B_4C nanoparticles were synthesized by milling of original B_4C powders with a mean size of 0·8 μm in an attrition mill (union process, model 1-S) using a hardened stainless steel vial and hardened stainless steel balls with 6 mm in diameter.

The ball to powder ratio and rotational speed were 15:1 and 400 rpm, respectively. Isopropyl alcohol was used as milling media and the grinding media occupied 80% of the chamber volume. The final mean size of the particles was 80 nm. After short blending stage of Al (96 wt %), B_4C (4 wt %) and adding 2 wt % of stearic acid as the process control agent (PCA), producing the composite powder of Al–4 wt % B_4C was done in a planetary high energy ball mill (Fritsch, model Pulverisette 6) and milling was performed in room temperature and under Argon gas atmosphere using a hardened steel vial and hardened steel balls with 20 mm in diameter, the ball to powder weight ratio and rotational speed being 10:1 and 350 rpm, respectively. To hinder overheating, ball milling experiments were paused periodically (every 1 h) and then resumed when the container temperature fell to room temperature. Powder samples were withdrawn at time intervals of 5, 10, 15 and 20 h for morphological and structural studies. The size of as-received and milled powders was quantified by a laser particle size analyser (Horiba LB 550). X-ray diffraction pattern of the powders in air atmosphere was taken by Siemens X-ray diffractometer (30 kV and 25 mA) using Cu Kα radiation. The peak broadening observed in XRD could be due to instrumental factor and physical factors such as crystallite size and lattice strain. The average crystal size and lattice strains were obtained using Williamson–Hall plot (Suryanarayana and Grant Norton 1998)

$$\beta_S \cos\theta = \frac{k\lambda}{d} + 2\eta \sin\theta, \tag{1}$$

where β_S, λ, θ, D and η are full width at half maximum (FWHM), the wavelength, peak position, crystal size and lattice strain, respectively. The instrumental broadening (β_i) was removed by applying the following equation

$$\beta_S = \beta_e^2 - \beta_i^2, \tag{2}$$

where β_e is the FWHM of the measured XRD peak.

The morphological characterization of the powders was studied by scanning electron microscopy (Philips-XL30). The milled powders were mounted, cross sectioned and polished in preparation for the microhardness and SEM analysis, then the distribution of the reinforcement within the powders was examined by a FE-SEM (Hitachi 4160F). Microhardness of powders was evaluated by Vickers method at a load of 25 g averaging 5–10 indents.

The Al and Al–4 wt % B_4C were cold pressed uniaxially in a cylindrical die at a range of 100–800 MPa. Compressibility behaviour of milled powders was followed by making compacts at different pressures. The density of samples was measured according to Archimedes' technique.

3. Results and discussion

3.1 *Morphology and particle size distribution of B_4C nanoparticles*

As received B_4C powder with a mean particle size of about 0·8 μm was used as the starting material. SEM micrographs of as received powder reveal that the powder has a wide size distribution and irregular shape (figure 1(a)).

Figure 1(b) shows the variation of particle size distribution and median size (D_{50}) as a function of milling time measured by a particle size analyser. By increasing the milling times, particle size decreases and a narrow size distribution is seen. During milling, a combination of fracture mechanisms occurs which include abrasion, compression and impact mechanism. The particle size distribution of a material after grinding will be determined by the combination of all mechanisms. The predominant mechanism is determined according to material properties and operating conditions. Since hard materials are difficult to be abraded on their surfaces, the impact mechanism plays a dominant role, thus, the distribution curve shows a monomodal distribution curve.This result is consistent with that reported by Shinohara *et al* (1999) regarding grinding of diamond. Figure 1(c) presents TEM image of the nanoparticles. The nanoparticles are spherical and have a uniform distribution. The XRD pattern, shown in figure 1(d), reveals the nanoparticles to exhibit the B_4C rhombohedral structure.

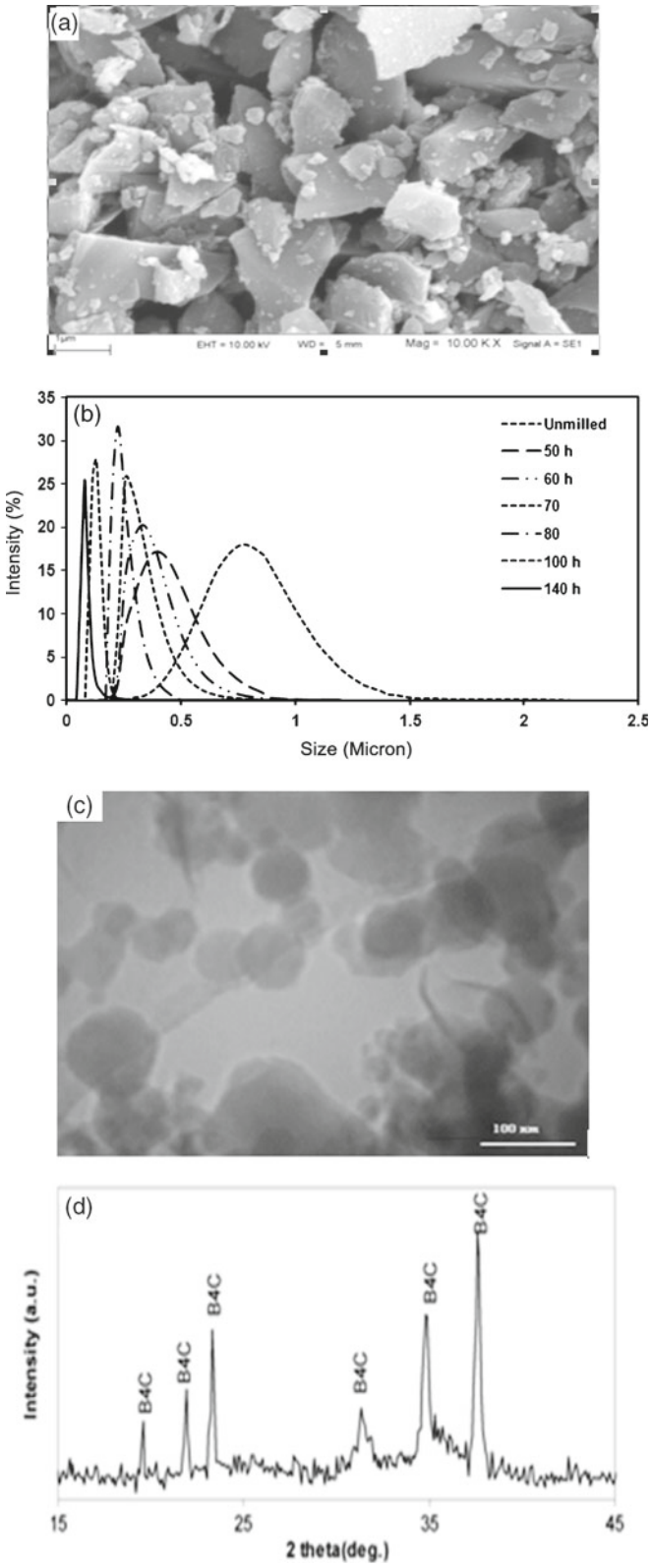

Figure 1. (**a**) SEM micrograph of as-received B_4C particles, (**b**) particle size distribution of ball milled boron carbide, (**c**) TEM micrograph of B_4C particles after 140 h milling and (**d**) XRD patterns of ball milled boron carbide particles.

3.2 *Preparation of Al–B_4C composite powder*

3.2a *Morphological and size analysis*: The Al particles are almost spherical in the initial stage (figure 2(a)) after milling for 5 h, the particles change into flake like ones. Also, the average size of the particles increases (figure 2(b)). The predominant mechanism in this stage is plastic deformation and cold welding. The former causes change in shape of the particles and the latter increases size and forms larger structures, the flake-like particles work harden after 10 h and as a result, the fracture mechanism is activated. The flake-like morphology remains unchanged after 10 h but the distribution and average size of the particles decreases (figure 2(c)). In fact, the large flaky particles fracture by drastic impacts. After increasing milling time to 15 h the powder morphology is not fully equiaxed (figure 2(d)). After 20 h milling, a lower aspect ratio can be observed and the size distribution of the particles becomes narrow (figure 2(e)). Increasing milling time for more than 20 h has no effect on powder morphology. In fact, at higher milling times, there occurs a steady state. It should be noted that after stabilizing the size of powder, the microstructure refinement still occurs and ends at a later time. Figure 3 shows morphology of the mechanically milled Al–4 wt % B_4C powder. The milling stages are partially similar to unreinforced Al, i.e. the plastic deformation of Al matrix to form flattened particles, welding the flake-like particles and fracture of particles. By considering the morphological changes, one can see the effect of reinforcement addition on MA process. It is obvious that welding, fracture and plastic deformation of Al matrix are affected by B_4C particles addition. Despite the ductile nature of the Al powder, because of the presence of B_4C particles, the large flake-like particles do not form. After 5 h milling (figure 3(a)), the resultant particles are not as flat as unreinforced Al. Because of presence of a ductile matrix like Al, the predominant mechanism is cold welding in this stage but presence of B_4C particles decreases the weldability of the Al powder. Thus, small irregular particles with a relatively low aspect ratio also result. By increasing the milling time to 10 h, one can see the gradual decrease in the aspect ratio of the irregular particles (figure 3(b)). After increasing the milling time to 15 h, equiaxed particles almost form and the particles have a stable shape and size distribution (figure 3(c)). Milling for times higher than 20 h have no effect on the morphology (figure 4(d)). It is clear that presence of B_4C particles makes the milling time faster and also decreases the time needed to reach steady-state.

The effect of milling time on the particle size of unreinforced Al and composite powder is shown in figure 4. The average particle size of unreinforced Al has a maximum at 5 h milling indicating formation of particles; the predominant mechanisms in this stage are particle deformation and cold welding. At longer milling times, fracture mechanism is predominant and the particle size decreases and finally the unreinforced Al powder reaches a steady state at 20 h which may be due to equilibrium condition between fracture and

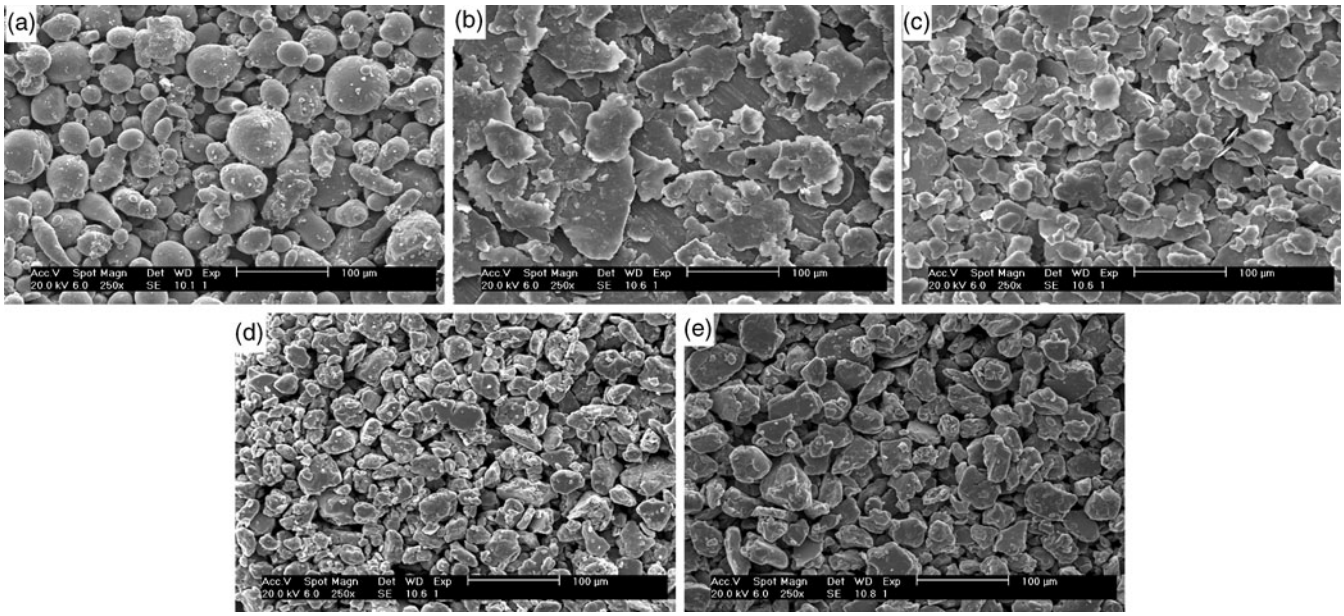

Figure 2. Morphology of unreinforced Al after (**a**) 0 h, (**b**) 5 h, (**c**) 10 h, (**d**) 15 h and (**e**) 20 h milling.

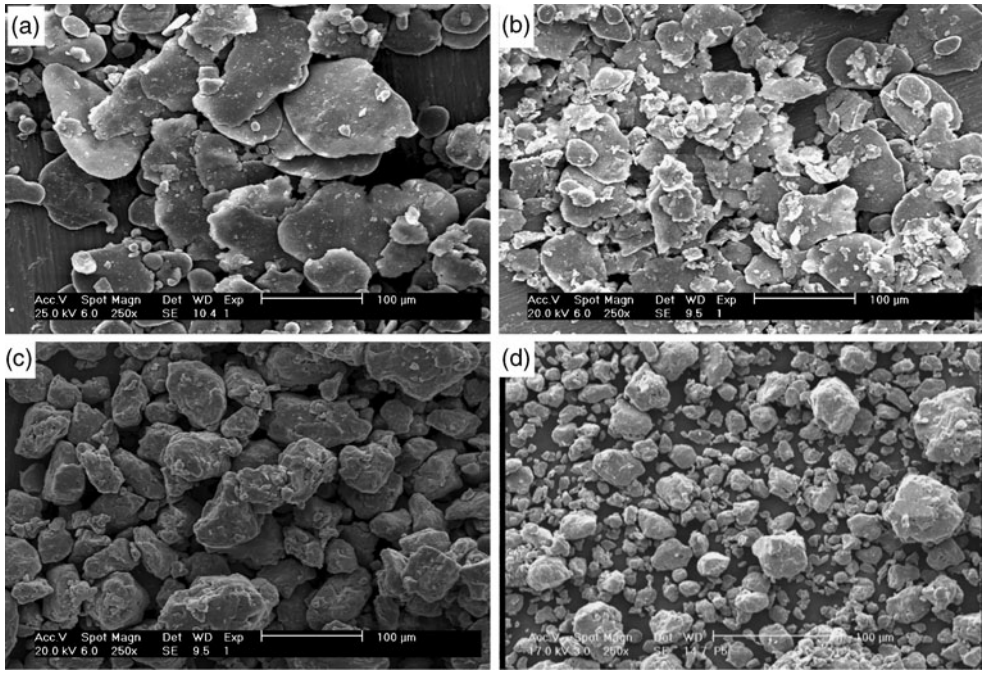

Figure 3. Morphology of composite powder after (**a**) 5 h, (**b**) 10 h, (**c**) 15 h and (**d**) 20 h milling.

welding. By adding B_4C particles to Al powder, the time needed to reach steady state reduces to 15 h.

In fact, the presence of B_4C particles within an individual Al particle resembles the microstructure of a typical particulate reinforced metal matrix composite (MMC). It is known that the stages of milling in metal matrix composite powders include plastic deformation of the ductile matrix, fragmentation of brittle particles, welding and fracture of the deformed particles (Suryanarayana 2001; Fogagnolo *et al* 2003). As compared to the MA of soft powders, the presence of hard particles causes an increase in local deformation of the matrix around the reinforcing particles. They would also enhance the work hardening rate of the matrix. Additionally, the fracture toughness of composite powders is lower than that of the matrix material. The possible reasons for the lower fracture toughness of MMCs include (i) altered slip

characteristics, (ii) increased strain to failure at crack tip due to the presence of hard particles and (iii) increased yield point (Davidson 1991). In other words, the small hard particles in matrix act as small milling agents. Therefore, the fracture process begins sooner in mechanical alloying of composite powder and the time needed to reach steady state decreases. A similar behaviour was observed by Abdoli *et al* (2008) in studying the ball milling of Al–AlN system.

A possible scheme of the mechanical milling process has been proposed in figure 5 (Fogagnolo *et al* 2003). In the early stage of milling, the ductile particles are deformed while some brittle particles undergo fragmentation. Then, when ductile particles start to weld, the brittle particles enter the soft powder to form a flattened composite powder. Because welding is the predominant mechanism in the process, the particles change their morphology by accumulating laminar particles. With the milling time prolonged, the ability of the particle to accept further plastic deformation was diminished; thus, fracturing became a significant process. Welding and fracture mechanisms then reach equilibrium, promoting the formation of composite particles with randomly orientated

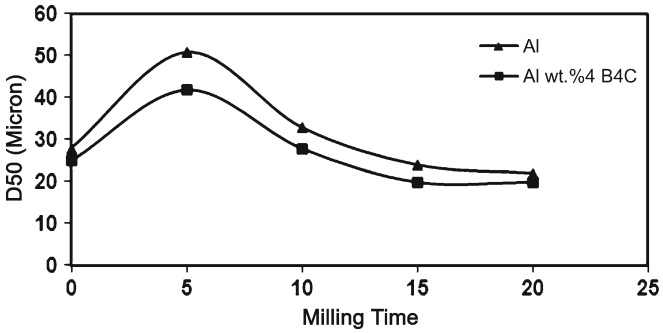

Figure 4. Effect of milling time on average particle size of monolithic and composite powders.

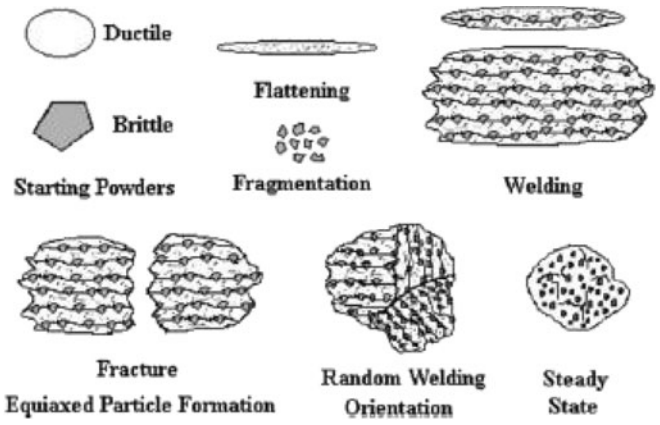

Figure 5. Various stages of ductile-brittle system during mechanical milling.

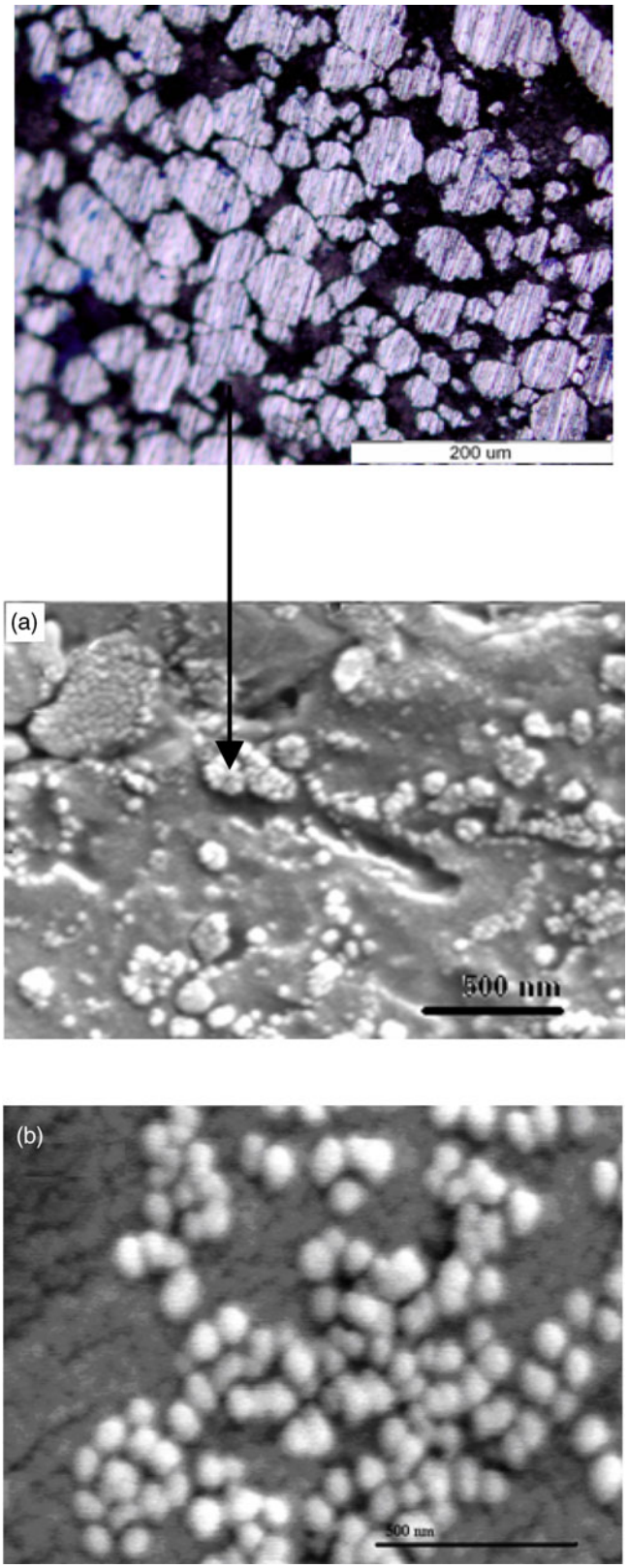

Figure 6. (**a**) Cross sections (mounted in epoxy resin matrix) of powders milled (darker region around particles is resin). Distribution of boron carbide particles within the Al matrix with milling time after (**b**) 10 h and (**c**)15 h.

interfacial boundaries. At the steady state, the microstructure undergoes a great refinement, and the interfacial boundaries are no longer visible by optical microscopy.

3.2b *Structural evolution*: Figure 6(a) shows optical image of the cross-section of mechanically milled powders and figure 6 (b and c) show SEM micrographs of B_4C dispersion in Al matrix after MA for different times. It can be seen that reinforcing B_4C particles disperse homogenously with increasing mechanical alloying time. After 10 h milling, clusters of B_4C particles were observed (figure 6(b)) that result from the large size difference between Al powder and B_4C particles and short time of MA. Compared to 10 h MA, with increasing milling time to 15 h, a full homogenous distribution of B_4C particles in matrix can be seen (figure 6(c)). Comparing figure 6 with figure 3(b and c), it can be concluded that steady state has a vigorous dependence on size distribution of B_4C particles in Al matrix. Thus, steady state takes place only when full homogenization of reinforcing particles in the matrix exists.

Figure 6 shows the dependence of apparent density on milling time for Al and reinforced powder. For both unreinforced Al and composite powder three stages can be seen; decrease, increase and finally steady state. Spherical morphology of as-received Al powder causes improved packing (figure 7(a)), thus it has an increased apparent density. At short milling times, there was a continuous decrease in the apparent density with a minimum between 5 and 10 h. This decrease can be attributed to the formation of flake like particles (figure 2(b)) and as a result, packing properties of powders are degraded. After longer milling the powder particles are work hardened and fractured. Thus spherical particles form and packing properties improve. After milling for 20 h, no changes can be seen in the apparent density. At this milling time, a balance between welding and fracture takes place. As it is confirmed by SEM micrographs, this is because steady state is reached. The apparent density evolution with milling time for composite powder is similar to that of Al powder, but in the presence of reinforced powder, the apparent density behaviour occurs in a shorter time so that after 15 h milling, no changes occur in apparent density as it can be seen in SEM micrographs.

The result of dividing the principal (111) and secondary (200) reflection of Al in XRD pattern at different milling times is shown in figure 8. The dependence of I (111) /I (200) ratio on milling time is very analogous to that of apparent density. It falls to a minimum then increases to reach steady state. This process is faster for composite powder. Similar results were observed for I (111) /I (200) ratio with milling time by Amador and Torralba (2003). This can be understood by considering the anisotropy in elastic modulus of a single crystal, Al. Therefore, the grains inside particles are deformed to thin layers in soft direction, vertical to the direction to which the particles are flattened by ball milling. When the sample is prepared to perform the powder XRD analysis, this flattened powder and its (200) planes are arranged parallel to sample holder and as a result I (200) increases while I (111) decreases. By more milling, flattened particles fracture and divide into equiaxed particles. So, particles lose their texture or preferential orientation and their reflection planes randomly arrange again and I (111) reflection recovers its significance. Figures 9 and 10 show XRD pattern of milled powders for different milling times, revealing the structural evolution of the powder mixture as the milling process progressed. When milling time increases, the peaks are gradually broadened and their intensities decreased. This noteworthy phenomenon i.e. peak broadening, is due to a decrease in crystallite size and an increase in lattice micro-strain. The crystallite size and the lattice strain are calculated from Williamson–Hall plots. They are plotted versus milling time in figure 11. This can be seen that the calculated crystallite size decreases rapidly in the initial stage of milling and as milling time increases, steady state occurs in a shorter time. Furthermore, addition of B_4C particles makes the grain size finer. Grain size remaining constant is due to a balance between the grain refinement produced by severe plastic deformation of milling and recovery through thermal process. Increasing the grain

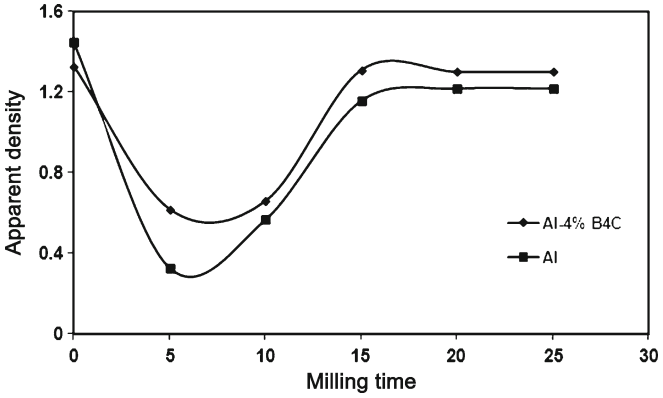

Figure 7. Apparent density versus milling time for unreinforced and composite powders.

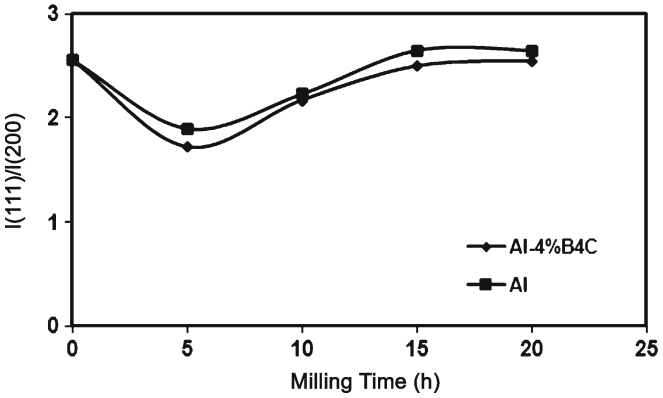

Figure 8. Effect of milling time on I (111)/I (200) ratio of Al in case of unreinforced and composite powders.

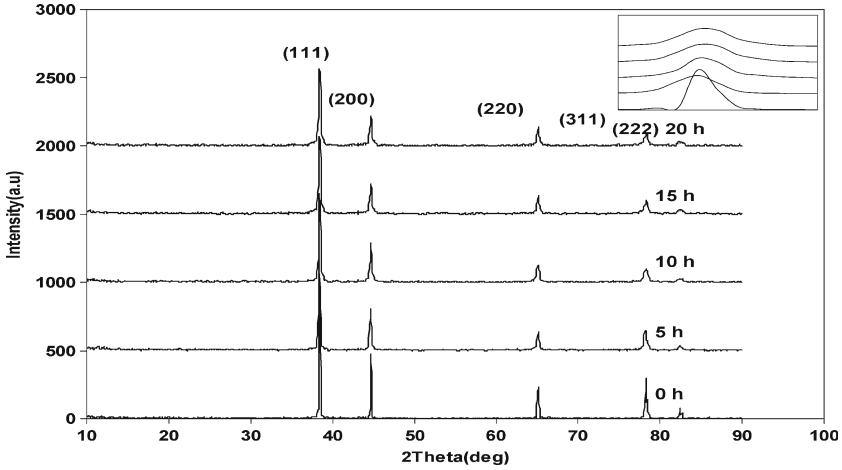

Figure 9. XRD patterns of Al powder milled for 0, 5, 10, 15 and 20 h.

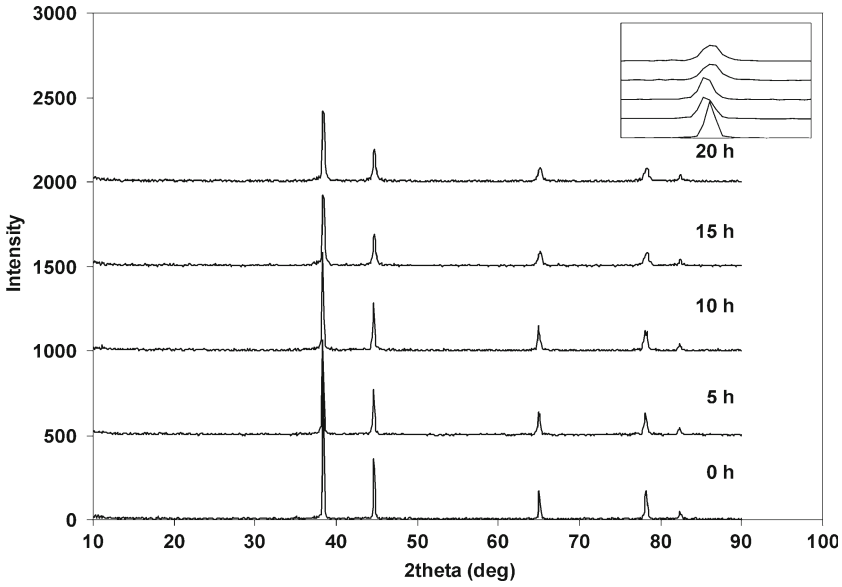

Figure 10. XRD patterns of composite powders milled for 0, 5, 10, 15 and 20 h.

refinement during MA process can be construed based on the dislocation formation mechanism via cyclic loading and also by thermal expansion coefficient mismatch between matrix and reinforcement. There is an interaction between these dislocations with nanoscaled particles which generates sub-boundaries. The sub-boundaries in turn cause the decomposition of initial large grains into smaller ones. The reduced size of the Al grain when milled at the presence of small size B_4C particles which are hard and difficult to deform can be partially ascribed to hindering of the movement of the dislocation by Orowan strengthening mechanism, resulting in increased dislocation density and thus accelerating the grain refinement process. The microhardness changes with milling time for unreinforced Al and composite powder is shown in figure 12. Both the unreinforced Al and composite powder show increasing hardness with milling time. By combining the famous Hall–Petch equation and Tabors empirical relationship, $H = 3\sigma$, it can be said that the nanostructured Al matrix influences the strength according to the following equation

$$H = H_0 + K D^{-1/2}, \tag{3}$$

where H_0 and k are appropriate constants associated with the hardness measurement and D the size of crystallite.

The difference between hardness of unreinforced Al and composite powder is due to the presence of B_4C particles and Orowan strengthening mechanism. The Orowan strengthening effect is produced by the interaction of dislocations and

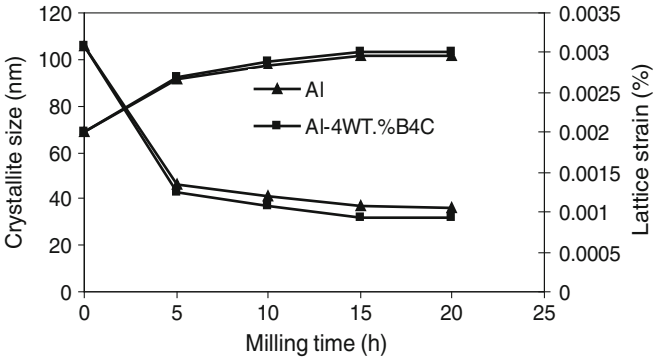

Figure 11. Crystallite size and lattice strain of unreinforced Al and composite powders vs milling time.

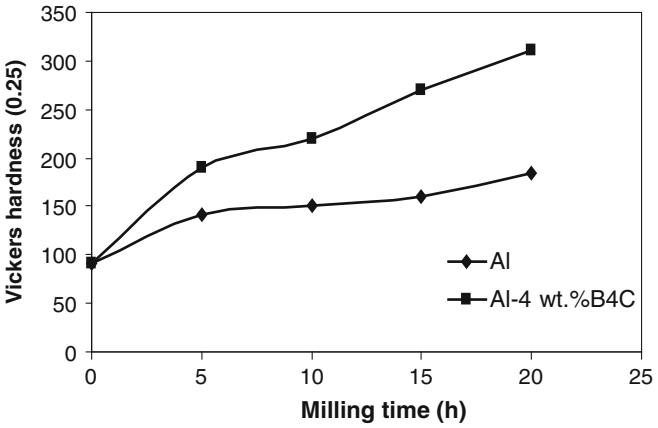

Figure 12. Powder hardness of monolithic and reinforced Al vs milling time.

Table 1. Fitting constants obtained from modified Heckel equation.

Material	D_0	σ_0	ν	R^2
Al	0·6178	91·54	0·2734	0·9911
Al–4 wt % B_4C	0·6161	171·2	0·2611	0·9927

impenetrable particles according to the following equation (Moona *et al* 2008)

$$H_{\mathrm{Oro}} = 3\sqrt{3}\frac{Gb}{\lambda}, \tag{4}$$

where G and b are shear modulus of matrix and Burgers vector, respectively and λ the interparticle spacing between dispersoids.

3.2c *Compressibility behaviour*: Cold compaction behaviour of 20 h milled Al and Al–4 wt % B_4C was studied. It can be said that their behaviour were in good agreement with modified Heckel equation.

Heckel (1961) showed that increasing relative density obeys a first order type of reaction with compaction pressure

$$-\frac{dD}{dP} = K\,(1 - D). \tag{5}$$

The slope K is in relation with the yield strength (σ_0) of the material in the following way

$$K = 1/3\sigma_0. \tag{6}$$

This resulted in the following equation which correlates relative density to applied pressure

$$\ln\left(\frac{1}{1-D}\right) = \ln\left(\frac{1}{1-D_0}\right) + \frac{P}{3\sigma_0}, \tag{7}$$

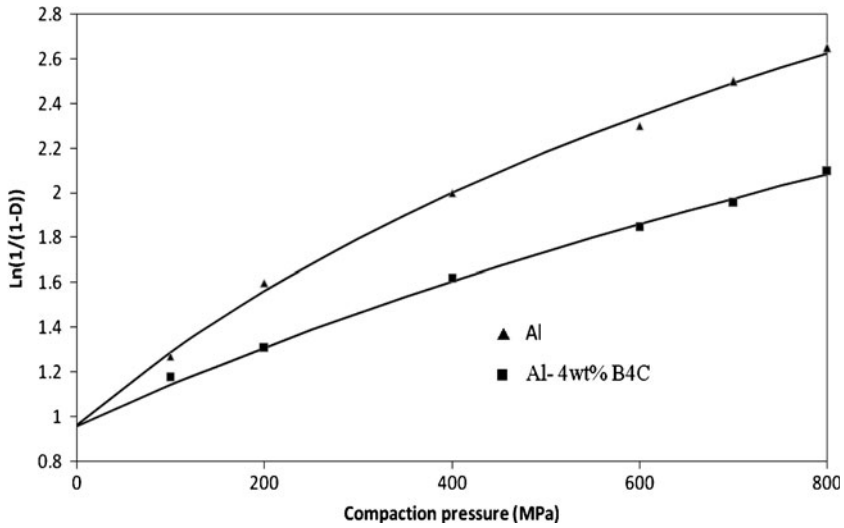

Figure 13. Relative density vs compaction pressure fitted to modified Heckel equation for unreinforced Al and composite powders.

where D_0 is the relative density at P equal to zero. In order to show the dependence of yield strength on pressure, a linear equation was applied

$$\sigma = \sigma_0 + K_1 P, \tag{8}$$

where σ is yield strength of compacts and σ_0 the yield strength of examined material at zero pressure. This equation explains that as the compaction reduces the volume fraction of porosity and the neighbouring particles cause increasing constraint (Peter Martin *et al* 2007).

The following equation can be obtained by substituting (8) and (6) in (5) and integrating

$$\ln\left(\frac{1}{1-D}\right) = \ln\left(\frac{1}{1-D_0}\right) + \frac{1}{3K_1}\ln\left(1+\frac{K_1 P}{\sigma_0}\right). \tag{9}$$

In order to reach yield strength of the material, the applied stress must be increased by

$$K_1 = \frac{2\nu^2}{1-2\nu}, \tag{10}$$

where ν is poissons ratio.

Within the die there are axial and radial pressures that by considering them and assuming a perfectly rigid die, Denny (2002) proposed the above equation.

Equations (7) and (9) were used to fit experimental data for both reinforced and unreinforced powders and are shown in figure 13.

The constants of equation were obtained and are given in table 1. The ν constant is in the range of metallic materials (i.e. about 0·33).

It is known that composite powders follow a behaviour similar to unreinforced metals under compaction. Addition of hard B_4C particles led to decreasing compressibility of the milled powders. In fact, densification of composite system is inhibited because it requires extra deformation in soft particles to fill the voids among the hard inclusions of reinforcements (Jiang *et al* 2000). The steeper slope of composite curve confirms this fact.

4. Conclusions

Boron carbide nanoparticles can be produced by attrition mill of commercially available (0·8 μm) boron carbide. The morphological and structural changes of unreinforced Al and Al–4 wt % B_4C mixture during ball milling stages was investigated and studied. It was found that the milling stages include plastic deformation, welding and fracture of particles.

The presence of hard ceramic B_4C particles accelerates the fracture. It is because of higher deformation applied to aluminum powder. As a result, formation of equiaxed particles i.e. steady state condition, was obtained after shorter milling time in comparison with unreinforced Al. This result was shown by correlation between apparent density vs milling time explained by the morphological and microstructure of the powder particles.

The distribution of boron carbide particles in the aluminum matrix reaches a full homogeneity when steady state takes place. MA process and presence of nanometer boron carbide particles increase the hardness of powder.

The compressibility behaviour of powders was studied after mechanical milling. The modified Heckel equation was used in order to consider the effect of applied pressure on yield strength and its trend explains the effect of compaction pressure. Addition of hard B_4C particles led to decreasing compressibility of the milled powder. Meanwhile, this effect resulted in higher yield strength for composite compacts for all levels of applied pressure.

References

Abdoli H, Salahi E, Farnoush H and Pourazrang K 2008 *J. Alloys Compd* **461** 166

Alizadeh A, Taheri-Nassaj E and Ehsani N 2004 *J. Eur. Ceram. Soc.* **24** 3227

Amador D R and Torralba J M 2003 *J. Mater. Process. Technol.* **143–144** 776

Aparecida M, Dos Santos P and Costa A 2006 *Powder Technol.* **169** 84

Boey F Y C, Yuan Z and Khor K A 1998 *Mater. Sci. Eng.* **A252** 276

Davidson D L 1991 *Mechanisms and properties*, in *Metal matrix composites* (eds) R K Everett and R J Arsenault (San Diego: Academic Press) p. 217

Denny P J 2002 *Powder Technol.* **127** 162

Fogagnolo J B, Velasco F, Robert M H and Torralba J M 2003 *Mater. Sci. Eng.* **A342** 131

Fogagnolo J B, Robert M H and Torralba J M 2006 *Mater. Sci. Eng.* **A426** 85

Gan K K and Gu M Y 2006 *Mater. Sci. Technol.* **22** 960

Heckel R W 1961 *Trans. Metall. Soc. AIME* **221** 671

Hu H M, Lavernia E J, Harrigan W C, Kajuch J and Nutt S R 2001 *Mater. Sci. Eng.* **A297** 94

Jiang G, Wu W, Daehn G S and Wagoner R H 2000 *Acta Mater.* **48** 4331

Jiang Q C, Wang H Y, Ma B X, Wang Y and Zhao F 2005 *J. Alloys Compd* **386** 177

Kerti I and Toptan F 2008 *Mater. Lett.* **62** 1215

Liua Y Q, Conga H T, Wanga W, Sun C H and Chenga H M 2009 *Mater. Sci. Eng.* **A505** 151

Mndoza-Ruiz D C, Esneider-Alcala M A, Guel E, Yoshida M, Lopez M and Martinez R 2008 *Rev. Adv. Mater. Sci.* **18** 280

Mohanty R M, Balasubramanian K and Seshadri S K 2008 *Mater. Sci. Eng.* **A498** 42

Moona O, Kim S, Jang J, Lee J and Lee C 2008 *Mater. Sci. Eng.* **A487** 552

Onoro J, Salvador M D and Cambronero L E G 2009 *Mater. Sci. Eng.* **A499** 421

Parvin N, Assadifard R, Safarzadeh P, Sheibani S and Marashi P 2008 *Mater. Sci. Eng.* **A492** 134

Peter Martin L, Hodge A M and Campbell G H 2007 *Scr. Mater.* **57** 229

Razavi Hesabi Z, Simchi A and Seyed Reihani S M 2006 *Mater. Sci. Eng.* **A428** 159

Saberi Y, Zebarjad S M and Akbari G H 2009 *J. Alloys Compd* **484** 637

Shinohara K, Golman B, Uchiyama T and Otani M 1999 *Powder Technol.* **103** 292

Suryanarayana C and Grant Norton M 1998 *X-ray diffraction: A practical approach* (New York: Plenum Press)

Suryanarayana C 2001 *Prog. Mater. Sci.* **46** 1

Wang L, Choi H, Myoung J and Lee W 2009 *Carbon* **47** 3427

Ye J, He J and Schoenung J M 2006 *Metall. Mater. Trans.* **A37** 3099

Zhang D L, Liang J and Wu J 2004 *Mater. Sci. Eng.* **A375** 911

Zhang H, Ramesh K T and Chin E S 2004 *Mater. Sci. Eng.* **A384** 26